Are Multi-electrode Arrays able to Differentiate Anatomical from Functional Reentries in an Excitable Sheet?

Laura Martínez[1], José Jalife[2], Omer Berenfeld[2], Javier Saiz[1]

[1]Ci2B, Universitat Politècnica de València, Valencia, Spain
[2]Center for Arrhythmia Research, University of Michigan, Ann Arbor, Michigan, USA

Abstract

Atrial fibrillation (AF) is one of the most common cardiac arrhythmias seen in clinical practice. Anatomical and functional reentries seem to be important in driving AF. Therefore, it is of great importance to identify and locate them. Multi-electrode array systems are increasingly being used to map the atrial electrical activity in humans. We use here computer simulations of reentries and process electrograms to perform phase maps, phase singularity (PS) detections and dominant frequency (DF) maps, in order to study if the multi-electrode array systems can distinguish properly between anatomical and functional reentries. Our results show that although there is no difference between phase maps corresponding to anatomical and functional reentries (all they exhibit rotors and therefore, in all cases a trajectory is tracked through the PS detections), overlapping the trajectories with the DF maps obtained it is able to distinguish anatomical from functional reentries.

1. Introduction

Atrial fibrillation (AF) is one of the most common cardiac arrhythmias seen in clinical practice [1-2]. Nevertheless, the mechanisms maintaining AF are still poorly understood, although both anatomical and functional reentries seem to be important in driving AF. Therefore, it is of great importance to identify and locate them with the new developed technologies in order to help physicians to improve treatment procedures, and thereby yield a better quality of life for patients.

Lately, the multi-electrode array systems are increasingly being used to map the atrial electrical activity in humans, with the aim of reconstructing spatio-temporal maps to be used as a tool for the diagnosis during ablation procedures [3-4]. An example of this is the group of Narayan, who were focused in mapping the atria to identify focal sources as well as rotors during AF in order to improve the ablation procedures [5-6].

We use here computer simulations to study if by using multi-electrode array systems it is possible to distinguish properly between anatomical and functional reentries.

2. Methods

2.1. Computer simulations

In order to study the ability of the multi-electrode arrays to distinguish between functional and anatomical reentries, we performed computer simulations in three different 3D sheets of dimensions 4.98 cm × 4.98 cm × 0.03 cm, corresponding to left atrial (LA) tissue (Sim1), pulmonary veins (PV) tissue (Sim2) and mitral valve ring (MVR) tissue (Sim3). The geometrical mesh consist of 27,556 hexahedral elements for Sim1, 26,612 for Sim2 and 23,916 for Sim3, with a spatial resolution between nodes of 0.03 cm. The geometrical mesh built to simulate the reentry around the PV contains a hole of 1 cm of diameter, while the mesh for the reentry around the MVR contains a hole of 2 cm of diameter, corresponding to experimental data [7], as shown in Figure 1.

Figure 1. Geometrical mesh for simulations of: A) LA (Sim1); B) PV (Sim2); C) MVR (Sim3).

Simulations in paroxysmal AF (pAF) conditions were carried out to reproduce a functional reentry in the left atrium (LA) and an anatomical reentry around a pulmonary vein (PV) and the mitral valve ring (MVR). The Courtemanche et al. model [8], modified by the I_{KACh} ionic current of the Grandi et al. model [9], was used to reproduce the cellular electrical activity under pAF conditions. In order to emulate the atrial regional electrophysiological heterogeneity, the maximum conductance of different ionic channels was modified to adjust the action potential duration to 90% of repolarization (APD_{90}) observed experimentally [10-11], as shown in Table 1. On the other hand, the I_{K1} was increased by 200% [12] to reproduce the electrical

remodeling in the LA regions observed in experimental studies (Table 1).

Table 1. Changes in the ionic currents of the model due to atrial heterogeneity and electrical remodeling

Electrophysiological Heterogeneity			
Changes in ionic currents [a]	***LA***	***PV***	***MVR***
I_{Kr}	1.60	2.40	2.44
I_{CaL}	-	-	0.67
Electrical remodeling under pAF conditions			
I_{K1}		2.00	

a. adimensional multiplicative factor w.r.t. values in [8]

Electrical activity was initiated by applying a cross-field stimulation protocol S1-S2, S1 being a planar stimulus applied at the lower edge of the tissue and S2 a square stimulus applied at the bottom left corner of the tissue.

The electrical propagation of action potentials (AP) in the tissue was obtained by solving the mono-domain reaction-diffusion equation (1) with the finite elements method [13], where D is the conductivity tensor (D_e extracellular and D_i intracellular), V_m the membrane potential, C_m the membrane capacitance and I_{ion} the sum of all the ionic currents flowing through the membrane.

$$\nabla \cdot (D\nabla V_m) = C_m \frac{\partial V_m}{\partial t} + I_{ion} \quad (1)$$

$$D = \frac{\lambda}{1+\lambda} \cdot D_i \quad (2)$$

$$\lambda = \frac{D_e}{D_i} \quad (3)$$

2.2. Calculation of extracellular potential

Extracellular electrical potentials (φ_e) were calculated by an approximation of the bidomain model in two steps. In the first step the V_m was computed by the monodomain model equation (1), as explained in 2.1. In the second step, φ_e was computed by using V_m as input for the second bidomain model equation (4), with the finite element method and Neumann boundary conditions [14].

$$\nabla \cdot (D_i \nabla V_m) + \nabla \cdot ((D_i + D_e)\nabla V_e) = 0 \quad (4)$$

For this, the computed V_m were interpolated onto a finite-element tetrahedron mesh of dimensions 4.95 cm × 4.95 cm × 4.86 cm containing two regions: a sheet of excitable atrial tissue with thickness of 0.09 cm, and a block of blood with thickness of 4.77 cm (Figure 2).

Unipolar electrograms (EGMs) were computed through the φ_e calculation on the coordinates where the electrodes forming the virtual multi-electrode contact array were located. Inter-electrode distance was set at 0.9 mm. Then EGMs were linearly interpolated (spatial resolution of 0.3 mm) to obtain a better visualization of the phase maps and a more accurate detection of the phase singularities (PS).

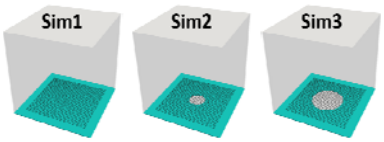

Figure 2. Tetrahedral meshes built for the EGM calculation: tissue (blue), blood (white) and multi-electrode array (black dots).

2.3. Interpolated phase maps

Once the EGMs were interpolated, phase maps were built based on the Hilbert transform [15-16]. The instantaneous location of a rotor, i.e. a functional reentry, can be given by PS at sites exhibiting [17-18]:

$$\oint \nabla\theta \cdot dr = \pm 2\pi, \quad (5)$$

where $\nabla\theta$ is the gradient of the instantaneous phase along a closed path surrounding the possible pivoting point. Points satisfying (5) were used to detect the rotors and its meandering.

2.4. Dominant frequency maps

The interpolated EGMs were processed in order to compute the dominant frequency (DF) maps as in [19], being the DF defined as the frequency corresponding to the highest peak of the power spectrum.

3. Results

After applying the cross-field stimulation protocol, three different reentries occurred: one of them functional in LA (Sim1) and the rest anatomical, being around PV (Sim2) and MVR (Sim3), as shown in the first column of Figure 3.C.

In Figure 3.A and Figure 3.B are depicted the V_m and EGMs registered on the black dot drawn in Figure 3.C, respectively. The cycle length (CL) of the V_m signals was calculated as the mean of the interval between excitations on that node. The CL ranged between 105.21ms and 131.96ms for the functional reentry in the LA (Sim1), between 107ms and 122ms for the anatomical reentry around the PV (Sim2) and between 148ms and 149ms for the anatomical reentry around the MVR (Sim3), being the mean 114.97ms, 112.75ms and 148.13ms respectively. The frequency of the electrical activation on that node, computed as the inverse value of the time interval between excitations, ranged between 7.57 and 9.51 Hz for Sim1, between 8.20 and 9.35 Hz for Sim2 and between

6.71 and 6.76 Hz for Sim3. The mean of the activation frequency was 8.72 Hz for Sim1, 8.88 Hz for Sim2 and 6.75 Hz for Sim3.

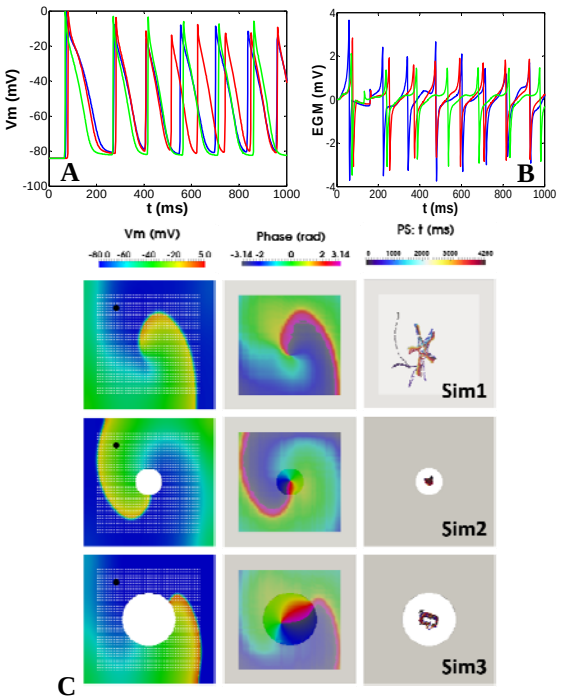

Figure 3. A-B) V_m and EGM in LA (blue), PV (red) and MVR (green), respectively; C) V_m (first column), phase maps (second column) and PS detections (third column) obtained for Sim1, Sim2 and Sim3. White dots on the first column images correspond to the multi-electrode array, and black dots to the node where signals in A and B were depicted.

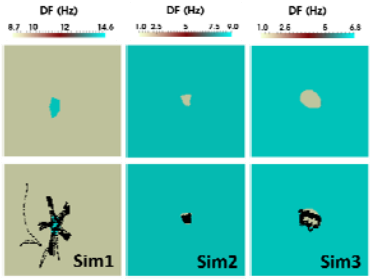

Figure 4. First row: DF maps computed for the functional reentry in the LA (Sim1) and the anatomical reentry around the PV (Sim2) and the MVR (Sim3). Second row: trajectories overlapped to DF maps.

Phase maps generated by the recordings of the multi-electrode array exhibited the anatomical reentries as rotors, and therefore a meandering was detected (second and third column of Figure 3.C). In case of the functional reentry (Sim1) the trajectory was detected in the tissue. However, in case of both anatomical reentries (Sim2 and Sim3), the trajectories were located spatially inside the hole, where there was no tissue.

Regarding the DF maps, for the functional reentry in the LA (Sim1) highest frequencies were located in the middle of the meandering area. However, for the anatomical reentries (Sim2 and Sim3) the meandering area coincided with the lower frequencies region and in addition, it was located in the middle of the hole. As shown in Figure 4, the DF ranged between 8.7-14.6 Hz for Sim1, 1-9 Hz for Sim2 and 1-6.8 Hz for Sim3.

4. Discussion

The results regarding phase maps show that either, functional and anatomical reentries, are registered by the multi-electrode array as a rotor, i.e. as a functional reentry, and also their meandering can be detected through the PS detections. In the anatomical reentries the trajectory is more concentrated spatially, while in the functional reentry it is wider. This is probably due to the effect of the hole around which reentry occurs. Phases existing in the edge converge inside and form a false PS, always located within the edge of the hole, and therefore anatomical reentries seem to be a rotor.

On the other hand, the CL of functional reentries is expected to be shorter compared to anatomical reentries [20]. In our study, the CL mean value is clearly shorter for the functional reentry than for the anatomical reentry around the MVR (114.97ms vs. 148.13ms). However, in case of PV the CL is shorter than in the functional reentry (112.75ms vs. 114.97ms). One reason for that results could be the fact that they are different tissues (LA, PV and MVR) and as a consequence the conduction velocity (CV) is also different, as well as the diameter of the hole.

Otherwise, paying attention to the results obtained from the DF maps in combination with those resulting from the PS detection, we observe how in a functional reentry, the trajectory location coincides spatially with the region where frequencies are highest, as expected [21] since the core of a rotor has shorter CV and APD_{90} than the tail, implying also a shorter CL and therefore a higher frequency of activation [20]. However, in case of anatomical reentries the trajectory coincides with the region of lowest DF (region inside the hole where there is any excitable tissue). Moreover, maximal DF are higher in the functional reentry than in the anatomical reentries (14.6 Hz vs. 9 Hz and 6.8 Hz). Thereby, although we detect a meandering in all cases, it is possible to differentiate the functional reentry from the anatomical due to the spatial coincidence of the trajectory with the highest DF region, since for anatomical reentries the trajectory coincides with the lowest DF region.

It would be of interest to perform further studies with a 3D realistic human atrial model and multi-electrode basket arrays, in order to check whether the results obtained with excitable tissue sheets are consistent with those obtained in the atria, where both the geometry and

the reentries are more complex. Furthermore, the inter-electrode distance would be non-equidistant in case of a 64-electrodes mapping basket catheter placed in the atria and the spatial resolution would be lower (in average approximately 20 mm for a basket with 5 cm of diameter), compared to the multi-electrode array system used in this study (spatial resolution of 0.9 mm, similar to that used in optical mapping). Therefore the interpolation of phases could produce false rotors [22].

5. Conclusion

Our results suggest that the multi-electrode arrays are very useful to detect reentries driving AF in an excitable sheet, thus combining phase and DF maps with PS detections they are able to distinguish whether a reentry is anatomical or functional.

Acknowledgements

This work was partially supported by the Programa Prometeo (PROMETEO/2012/030) from the Consellería d'Educació Formació I Ocupació, Generalitat Valenciana and the "VI Plan Nacional de Investigación Científica, Desarrollo e Innovación Tecnológica" from the Ministerio de Economía y Competitividad of Spain (TIN2012-37546-C03-01).

References

[1] Montes-Santiago J, Rodil V, Formiga F, Cepeda JM, Urrutia A. Features and costs of patients admitted for cardiac arrhythmias in Spain. Rev clínica española 2013;213(5):235–9.

[2] Fuster V, Rydén LE, Cannom DS, Crijns HJ, Curtis AB, Ellenbogen KA, et al. ACC/AHA/ESC 2006 guidelines for the management of patients with atrial fibrillation-executive summary. Eur Heart J 2006;27(16):1979–2030.

[3] Narayan SM, Krummen DE, Shivkumar K, Clopton P, Rappel WJ, Miller JM. Treatment of atrial fibrillation by the ablation of localized sources: CONFIRM trial. J Am Coll Cardiol 2012;60(7):628–36.

[4] Umapathy K, Nair K, Masse S, Krishnan S, Rogers J, Nash MP, et al. Phase mapping of cardiac fibrillation. Circ Arrhythm Electrophysiol 2010;3(1):105–14.

[5] Rappel WJ, Narayan SM. Theoretical considerations for mapping activation in human cardiac fibrillation. Chaos 2013;23.

[6] Narayan SM, Baykaner T, Clopton P, Schricker A, Lalani GG, Krummen DE, et al. Ablation of rotor and focal sources reduces late recurrence of atrial fibrillation compared with trigger ablation alone: extended follow-up of CONFIRM trial. J Am Col Cardiol 2014;63(17):1761–8.

[7] Cohen GI, White M, Sochowski RA, Klein AL, Bridge PD, Stewart WJ, et al. Reference values for normal adult transesophageal echocardiographic measurements. J Am Soc Echocardiogr 1995;8(3):221–30.

[8] Courtemanche M, Ramirez RJ, Nattel S. Ionic mechanisms underlying human atrial action potential properties: insights from a mathematical model. Am J Physiol Hear Circ Physiol 1998;275:301–21.

[9] Grandi E, Pandit SV, Voigt N, Workman AJ, Dobrev D, Jalife J, et al. Human atrial action potential and Ca2+ model: sinus rhythm and chronic atrial fibrillation. Circ Res 2011 Oct;109(9):1055–66.

[10] Li D, Zhang L, Kneller J, Nattel S. Potential ionic mechanism for repolarization differences between canine right and left atrium. Circ Res 2001;88:1168–75.

[11] Cha TJ, Ehrlich JR, Zhang L, Chartier D, Leung TK, Nattel S. Atrial tachycardia remodeling of pulmonary vein cardiomyocytes: Comparison with left atrium and potential relation to arrhythmogenesis. Circulation 2005;111:728–35.

[12] Voigt N, Trausch A, Knaut M, Matschke K, Varró A, Van Wagoner DR, et al. Left-to-right atrial inward rectifier potassium current gradients in patients with paroxysmal versus chronic atrial fibrillation. Circ Arrhythmia Electrophysiol 2010;3:472–80.

[13] Heidenreich EA, Ferrero JM, Doblaré M, Rodríguez JF. Adaptive macro finite elements for the numerical solution of monodomain equations in cardiac electrophysiology. Ann Biomed Eng 2010;38:2331–45.

[14] Keller DUJ, Weber FM, Seemann G, Dössel O. Ranking the influence of tissue conductivities on forward-calculated ECGs. IEEE Trans Biomed Eng 2010 Jul;57(7):1568–76. A

[15] Warren MD, Berenfeld O, Guha PK, Chen J, Samie FH, Zaitsev AV, et al. IK1 blockade reduces frequency, increases organization and terminates ventricular fibrillation in the guinea pig heart. PACE 2001;24(4,II):647

[16] Sarmast F, Kolli AK, Zaitsev AV, Berenfeld O, Jalife J. Acetylcholine induces a transition from right to left predominance in frequency of activity during atrial fibrillation in the goat. PACE 2002;25(4,II): abstract # 50.

[17] Bray M., Lin SF, Aliev RR, Roth BJ, Wikswo JP. Experimental and theoretical analysis of phase singularity dynamics in cardiac tissue. J Cardiovasc Electrophysiol 2001;12(6):716–22.

[18] Rogers JM. Combined Phase Singularity and Wavefront Analysis for Optical Maps of Ventricular Fibrillation. IEEE 2004;51(1):56–65.

[19] Tobón C, Ruiz-Villa CA., Heidenreich E, Romero L, Hornero F, Saiz J. A Three-Dimensional Human Atrial Model with Fiber Orientation. Electrograms and Arrhythmic Activation Patterns Relationship. PLoS One 2013;8(2).

[20] Jalife J. Déjà vu in the theories of atrial fibrillation dynamics. Cardiovasc Res 2011;89(4):766–75.

[21] Mansour M, Mandapati R, Berenfeld O, Chen J, Samie FH, Jalife J. Left-to-right gradient of atrial frequencies during acute atrial fibrillation in the isolated sheep heart. Circulation. 2001;103:2631–6.

[22] Berenfeld Omer OH. The Quest for Rotors in Atrial fibrillation: Different Nets Catch Different Fishes. Hear Rhythm. 2012;9(9):1440–1.

Address for correspondence:

Laura Martínez Mateu
Ci2B - Ciudad Politécnica de la Innovación, Cubo Azul Edif. 8B, Acceso N. Camino de Vera s/n, 46022 - Valencia (Spain)
laumarma@gbio.i3bh.es